Article

Pharmaceutical salts of biologically active hydrazone compound salinazid: crystallographic, solubility and thermodynamic aspects

Artem O. Surov, Alexander P. Voronin, Anna A. Simagina, Andrei V. Churakov, and German L. Perlovich

Cryst. Growth Des., **Just Accepted Manuscript** • DOI: 10.1021/acs.cgd.5b01681 • Publication Date (Web): 30 Mar 2016

Pharmaceutical salts of biologically active hydrazone compound salinazid: crystallographic, solubility and thermodynamic aspects

Artem O. Surov[a], *Alexander P. Voronin*[a], *Anna A. Simagina*[a], *Andrei V. Churakov*[b], *German L. Perlovich*[a,*]

[a]Institution of Russian Academy of Sciences, G.A. Krestov Institute of Solution Chemistry RAS, 153045, Ivanovo, Russia. E-mail: glp@isc-ras.ru

[b]Institute of General and Inorganic Chemistry RAS, Leninskii Prosp. 31,119991, Moscow, Russia.

*To whom correspondence should be addressed: Telephone: +7-4932-533784; Fax: +7-4932-336237; E-mail glp@isc-ras.ru

Abstract

The crystal structures of salts of the active pharmaceutical ingredient (API) called salinazid with dicarboxylic acids and acesulfame were determined by single-crystal X-ray diffraction method. The crystals contain hydrogen bond motifs of different structure and complexity, the energies in which were estimated by using the quantum theory of atoms in molecules and crystals (QTAIMC) methodology. It was found that the driving force for facile the oxalate and malate salts formation is the bifurcated N^+–H···O^- and N^+–H···O hydrogen bond synthon, while salinazid malonate is mainly stabilized via a "classic" pyridinium-carboxylate heterosynthon. The oxalate and acesulfame salts of salinazid were found to be stable during aqueous dissolution experiments, providing a substantial solubility improvement compared to pure API (33 and 18 times, respectively). However, the malonate and malate salts dissolved incongruently and rapidly underwent a solution-mediated transformation to form pure salinazid. Based on the solubility data of the stable salts and of the pure components, the Gibbs free energy of the salts formation were calculated to be -21.2 kJ·mol^{-1} for salinazid oxalate and -22.6 kJ·mol^{-1} for salinazid acesulfame.

Keywords: hydrazone derivatives; pharmaceutical salts; X-ray diffraction; solid-state DFT calculations; noncovalent interactions; solubility; formation thermodynamics.

1. Introduction

Selection of an appropriate dosage form for a drug compound is a crucial step in the process of drug development.[1] It has been reported that approximately 80% of all medications are delivered on the market as solid-state formulations (e.g., tablets, capsules, etc.) due to their evident advantages in terms of stability, longer storage, production and transportation economy, and convenience of the intake.[2-5] Pharmaceutical solids are classified as enteral drug forms. This implies the oral route of administration of the active pharmaceutical ingredient (API) and delivery through the gastrointestinal tract. However, pharmaceutically relevant physicochemical properties of an API, such as solubility, chemical and thermodynamic stability, bioavailability, etc., usually have to be modulated and tuned to provide the optimal API solid form for practical use. One of the straightforward ways to considerably improve the physicochemical and biological properties of an API without modifying its pharmacophore structure is to develop novel solid forms such as salts or co-crystals. It has been reported that salt formation is the most frequently chosen method in the pharmaceutical industry and today more than 50% of APIs are marketed as salts.[6] In the realm of salts, the main challenge to consider is selection of a suitable counter-ion, which would provide desired properties of a new solid form. For weakly basic APIs, salt formation with inorganic acids (such as hydrochloric acid) has often been the most obvious and convenient way to improve bioavailability of a drug. However, there are some potential drawbacks of using, for example, hydrochloride salts, namely, their high acidity in parenteral formulations, the risk of corrosion of industrial equipment, a decreased solubility in the stomach due to a common ion effect, etc.[7] These problems can be partly avoided by using pharmaceutically acceptable carboxylic acids and other relatively strong organic acids that are able to form stable co-crystal/salt forms with weakly basic APIs.[8]

This work is a continuation of our previous studies[9] concerning new crystalline forms of the biologically active hydrazone compound salinazid (**Slz**) ((2-hydroxybenzaldehyde)isonicotinoyl hydrazone) (Figure 1). Hydrazones represent a special group of Schiff base compounds, that are of a great interest to the pharmaceutical and medicinal chemistry because of broad spectrum of biological activities.[10,11] Hydrazone derivatives have been recognized as potent agents for treatment of drug-resistant forms of tuberculosis[12-14] and reported to have lower toxicity than isoniazid (an important first-line antituberculosis drug) due to the blockage of –NH2 group.[15] Moreover, the methoxy- and hydroxy- substituted hydrazones have been demonstrated to possess antioxidant[16] and antitumoral activities.[17]

In this work, we discuss the crystal structures and physicochemical properties of the salinazid salts with well-known pharmaceutically acceptable dicarboxylic acids, namely oxalic acid, malonic acid and malic acid (Figure 1). In addition, well known sugar substitute called acesulfame was used as a salt former. Acesulfame is an aliphatic calorie-free sweetener, and its potassium salt is widely used in food products and pharmaceutical formulations. It has been reported that organoleptic properties of a formulation can be improved by adding acesulfame, which suppress the bitter taste of a drug.[18] However, examples of using acesulfame as a guest molecule to prepare novel solid forms are limited. Multicomponent crystals containing acesulfame are currently described for the following drugs: griseofulvin,[19] haloperidol,[20] 5-fluorocytosine,[21] theophylline,[22] ciprofloxacin and norfloxacin.[23]

All the novel solid phases were characterized by X-ray diffraction and thermal techniques. Energies of the strongest intermolecular interactions in the crystals were estimated using the solid state DFT calculations with the subsequent quantum theory of atoms in molecules and

crystals (QTAIMC) analysis of the periodic electron density. Water solubility, stability and formation thermodynamics of the salinazid salts were also investigated and analyzed.

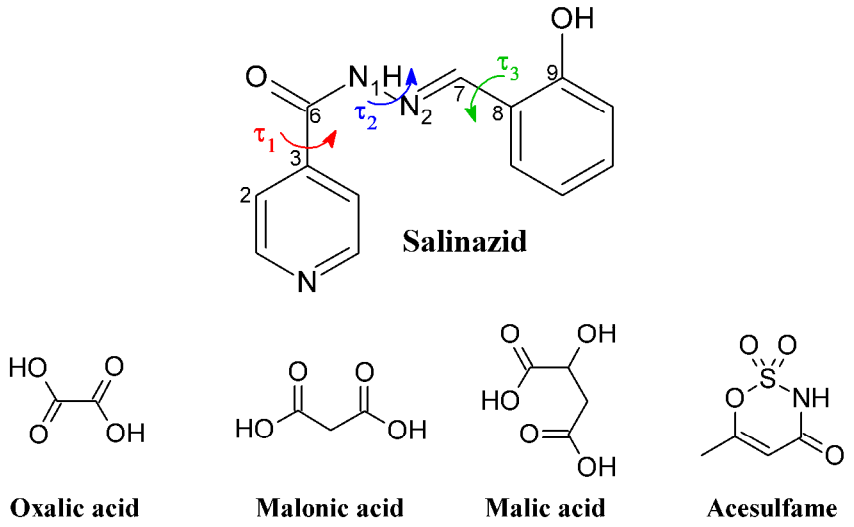

Figure 1. Molecular structures of salinazid, dicarboxylic acids and acesulfame used in this work. Flexible torsion angles in the salinazid molecule are numbered and indicated by τ_1, τ_2 and τ_3.

2. Material and Methods

2.1. Compounds and solvents

Salinazid ((2-hydroxybenzaldehyde)isonicotinoyl hydrazone, $C_{13}H_{11}N_3O_2$, 99%) was obtained from Interbioscreen Ltd. Oxalic acid dihydrate ($C_2H_2O_4 \cdot 2H_2O$, 99.5%) and acesulfame potassium ($C_4H_4KNO_4S$, 99%) were purchased from Sigma-Aldrich. Malonic ($C_3H_4O_4$, 99%) and DL-malic ($C_4H_6O_5$, 99%) acids were purchased from Acros Organics. All the solvents were of analytical grade and used as received without further purification. Acesulfame potassium was neutralized with HCl to obtain free acesulfame acid according to the procedure described by Velaga *et al.*[24] Acesulfame acid was identified as form I by X-ray powder diffraction (XRPD) and differential scanning calorimetry (DSC) (see Figure S1 of the supporting information).

2.2. Crystallization procedure

Due to considerable difference in solubilities of salt components in common organic solvents, a significant excess of acids (except for acesulfame acid) was needed to keep the conditions when only the salt is a thermodynamically stable solid phase. For the crystallization experiments of salinazid with malonic and malic acids, salinazid (50 mg, 0.2mM) and acids were dissolved in 10 ml of methanol in a 1:10 molar ratio and stirred at 50-60°C until a clear solution was obtained. The solution was slowly cooled and kept at room temperature. Diffraction quality yellow crystals of the malonate and malate salts appeared inside the solution over a period of 2-3 days.

An attempt to crystallize salinazid with oxalic acid using the same experimental condition as described above resulted in etherification of the acid molecule to form a hydrated salt of salinazid with monomethyl oxalate. The relevant crystallographic details and the asymmetric unit with displacement ellipsoids for this complex are given in the supporting information (Figure S2 and Table S1). Crystals of salinazid oxalate suitable for X-ray analysis were obtained after 2-3 days by slow evaporation of acetonitrile solution with the API to acid molar ratio equal to 1:2.

For the crystallization experiment of salinazid with acesulfame acid, equimolar amounts of components (0.2mM) were dissolved in 6 ml of methanol in a 1:1 molar ratio and stirred at 50-60°C until a clear solution was obtained. The resulting solution was allowed to crystallize at room temperature. Yellow crystals of acesulfame salt suitable for a X-ray experiment were collected in several days.

The bulk samples of the salts were obtained by slurring equimolar amounts of salinazid and corresponding acid in methanol (acetonitrile for salinazid oxalate) for several hours at room temperature.

2.3. X-ray diffraction experiments

Single-crystal X-ray diffraction data were collected on a Bruker SMART APEX II diffractometer using graphite-monochromated MoKα radiation (λ = 0.71073 Å) using ω-scan mode . Absorption corrections based on measurements of equivalent reflections were applied.[25] The structures were solved by direct methods and refined by full matrix least-squares on F^2 with anisotropic thermal parameters for all non-hydrogen atoms.[26] All hydrogen atoms were found from the difference Fourier map and refined isotropically. Data were collected at 183K for the crystals of [**Slz**+**Oxalic**] (1:1), [**Slz**+**Acesulfam**] (1:1) and at 150K for the [**Slz**+**Malonic**] (1:1), [**Slz**+**Malic**] (1:1) salts.

The crystallographic data have been deposited with the Cambridge Crystallographic Data Centre as supplementary publications under the CCDC numbers 1437855-1437859. This information may be obtained free of charge from the Cambridge Crystallographic Data Centre via www.ccdc.cam.ac.uk/data_request/cif.

X-ray powder diffraction (PXRD) data were recorded under ambient conditions in Bragg-Brentano geometry by a Bruker D8 Advance diffractometer with $CuK\alpha_1$ radiation (λ = 1.5406 Å).

2.4. DSC experiments

Thermal analysis was carried out using a Perkin Elmer DSC 4000 differential scanning calorimeter with a refrigerated cooling system (USA). Approximately 1-2 mg of the solid sample was heated in sealed aluminum sample holders in the temperature range of 25−280 °C at the rate of $10°C \cdot min^{-1}$ in a nitrogen atmosphere. The unit was calibrated with indium and zinc standards. The accuracy of the weighing procedure was ±0.01 mg.

2.5 Aqueous dissolution.

The solubilities of the solids were determined by the shake-flask method at 25.0 ± 0.1°C. An excess of each sample was added into pyrex glass tubes with 10 ml of degassed water. After 24 hours the solid phase was filtered through 0.2 μm PTFE syringe filter, and the concentration of a compound in a solution was determined by UV−vis spectroscopy (Varian Cary 50) at the reference wavelength (330 nm). Residual solid materials at the end of the solubility experiments were collected and analyzed by using PXRD.

2.6 Phase solubility studies

Solubility studies were performed as described by Connors.[27] Excess amounts of salinazid were added to 2 ml of the aqueous solutions containing different concentrations of the corresponding acids. The samples were shaken at 25.0 ± 0.1°C to attain equilibrium (24 hours), an aliquot was filtered using a 0.2 μm filter (Rotilabo® syringe filter, PTFE). The drug assay was measured by UV−vis spectroscopy (Varian Cary 50) at the reference wavelength (330 nm).

2.7 Computational procedure

The CRYSTAL14 software[28] was used to perform the DFT calculations with periodic boundary conditions (solid-state DFT) at the B3LYP-D2/6-31G** level of theory. In the present study we explored a simplified approach. It is widely used for the description of the particular types of intermolecular interactions (conventional H-bonds and/or C-H…O contacts).[29-31] In this approach the crystalline wavefunction is computed using the experimental space group, lattice parameters and atom coordinates. The Bader analysis was performed with TOPOND14[32,33] and the energies of the particular noncovalent interactions, E_{int}, were evaluated according to Mata *et al.*[34] as

$$E_{int} = 0.429 \cdot G_b \text{ (in atomic units)} \quad (1)$$

It has been reported that equation (1) yields reasonable values of E_{int} for intermolecular interactions with different strength from strong charge-assisted hydrogen bonds to weak van-der-Waals contacts.[35-39]

3. Results and Discussion

It is widely accepted in the literature that whether an API and a guest molecule form a salt or co-crystal can be predicted in terms of the ΔpKa rule ($\Delta pK_a = pK_a^{(base)} - pK_a^{(acid)}$).[40-42] When the ΔpKa is greater than 3, the components tend to form a salt. If $\Delta pKa \leq 0$, a co-crystal is likely to be formed. In the ΔpK_a range between 0 and 3, however, the ionization state of molecules in a crystal remains hardly predictable. The pK_a value based on pyridine nitrogen for salinazid is found to be 3.6,[43] which is quite close to that of its structural precursor isoniazid (3.5). Considering the first ionization constants of the acid molecules used in this work, the ΔpKa values are equal to 2.3 for oxalic acid ($pK_{a,1}$ = 1.3), 0.8 for malonic acid ($pK_{a,1}$ = 2.8), 0.2 for malic acid ($pK_{a,1}$ = 3.4), and 1.6 for acesulfame acid ($pK_{a,1}$ = 2.0). It is evident that for all the considered drug/coformer pairs the ΔpK_a should be considered in the salt−co-crystal continuum. Therefore, the resulting ionization state of the components in the multicomponent crystal cannot be reliably predicted.

3.1 Crystal structures of the salts and pattern of intermolecular interactions

Relevant crystallographic details for all the studied crystalline complexes are given in Table 1. Protonation of the pyridine ring of Slz by acid groups of the salt formers was confirmed by the single crystal X-ray diffraction data. This was evidenced by the proton location, analysis of the C-O bonds length in the acid molecules and the C-N-C angle value in the pyridine ring.[40] For example, C-O, C=O bond distances of 1.30, 1.20 Å and angles of 117-118° indicate a neutral synthon, whereas an intermediate distance of 1.25 Å and a of 120-122° mean an ionized

pyridinium state.[44-47] This fact suggests that proton transfer in the studied crystals may be facilitated by the crystalline environment and/or crystallization solvent.[48,49]

Table 1. Crystallographic data for salinazid salts

	[**Slz**+**Oxalic**] (1:1)	[**Slz**+**Malonic**] (1:1)	[**Slz**+**Malic**] (1:1)	[**Slz**+**Acesulfam**] (1:1)
Crystal data				
Chemical formula	$C_{13}H_{12}N_3O_2 \cdot C_2HO_4$	$C_{13}H_{12}N_3O_2 \cdot C_3H_3O_4$	$C_{13}H_{12}N_3O_2 \cdot C_4H_5O_5$	$C_{13}H_{12}N_3O_2 \cdot C_4H_4NO_4S$
Crystal size (mm)	0.22 × 0.20 × 0.03	0.20 × 0.20 × 0.15	0.25 × 0.20 × 0.10	0.42 × 0.17 × 0.01
Fw	331.28	345.31	375.34	404.40
Crystal system, space group	Monoclinic, $P2_1/n$	Monoclinic, $P2_1/c$	Triclinic, $P\bar{1}$	Monoclinic, $P2_1/c$
Temperature (K)	183	150	150	183
a (Å)	19.295(4)	13.2240(8)	7.7100(15)	15.7874(18)
b (Å)	5.5361(11)	9.3797(6)	10.443(2)	7.9201(9)
c (Å)	27.666(5)	12.4908(8)	11.671(2)	14.7285(17)
α (°)	90	90	106.805(3)	90
β (°)	95.408(3)	101.213(1)	97.485(3)	107.129(2)
γ (°)	90	90	109.110(3)	90
V (Å^3)	2942.0(10)	1519.75(17)	823.3(3)	1759.9(3)
Z	8	4	2	4
μ (mm^{-1})	0.12	0.12	0.12	0.23
Data collection				
θ range (°)	1.23 – 27.00	2.68 – 27.99	1.88 – 26.00	2.70 – 26.99
total refl.	26648	13970	7009	15579
unique refl., R_{int}	6399, 0.035	3668, 0.021	3207, 0.017	3826, 0.029
refl. with $I > 2\sigma(I)$	5054	3177	2721	3042
Refinement				
No. of parameters	537	286	306	317
$R_1[I > 2\sigma(I)]$	0.038	0.038	0.037	0.034
wR_2 (all data)	0.092	0.112	0.101	0.091
Goof	1.03	1.05	1.04	1.03
$\Delta\rho_{max}$, $\Delta\rho_{min}$ (e Å^{-3})	0.29, -0.19	0.39, -0.22	0.79, -0.23	0.36, -0.39

The salinazid molecule has two donor and two acceptor sites suitable for hydrogen bonding (Figure 1). The pyridine nitrogen atom is capable of forming neutral or charge-assisted hydrogen bonds, while the site containing an amino group (N-H) and a number of nearby C-H groups are also able to interact with the highly electronegative atoms of neighbour molecules. The main acceptors of hydrogen bonding in the Slz molecule are the oxygen atom of the hydrazide group and hydroxyl oxygen attached to the phenyl ring. Additionally, the aromatic fragments of Slz can

participate in phenyl C-H···O contacts and other weak intermolecular interactions, which stabilize the crystal lattice. However, simple examination of the molecular packing arrangement based only on geometrical criteria cannot provide reliable information about the strength of intermolecular contacts, since the existence of a short contact between atoms does not imply by default presence of an intermolecular (noncovalent) interaction.[50] Beside that, even for strong hydrogen bonds the geometric criteria cannot provide the exact value of E_{int} but only its variation range. Therefore, the pattern of intermolecular interactions in the crystals has been additionally investigated in terms of the quantum theory of atoms in molecules and crystals (QTAIMC).[51,52] It has been reported that this method is one of the most applicable approaches to estimate the strength of interactions of different nature in a uniform manner that would be in good agreement with the experiment.[35-39] In the present paper, the QTAIMC analysis was utilized to evaluate the energies of H-bonds and C-H···O contacts and to compare the relative strength of different structural motifs of the intermolecular interactions in the crystals of the salts.

3.1.1 [**Slz**+**Oxalic**] (1:1)

Salinazid oxalate crystallizes in the monoclinic $P2_1/n$ space group with two conformationally distinct oxalate anions and two planar API cations in the asymmetric unit. The conformations of salinazid molecules are nearly identical, whereas the main differences are observed between the oxalate ions. In the first of the symmetry unequivalent molecules (mol. ***F*** - flat), the carboxyl groups lie approximately in the same plane, so the torsion angle ∠O2-C1-C2-O3 equals -164.6° (Figure 2b). In the second molecule (mol. ***T*** - twisted), the deprotonated carboxyl group is twisted in relation to the protonated one through the angle of ∠O6-C3-C4-O8 = -102.3° (Figure 2a). The CSD analysis (version 5.36, may 2015 update)[53] has shown that the "twisted" conformation of the oxalate ion is rare in crystal structures (Figure S3). Therefore, the

stabilization of this higher-energy conformation in a crystal requires a considerable amount of non-covalent interaction energy. From X-Ray data one can observe that oxygen atoms of the twisted carboxylic group are located in proximity to the hydrazide N-H and several C-H groups of both symmetry independent **Slz** molecules (Figure 2a). The QTAIMC analysis confirms that the total energy of hydrogen bonds and C-H...O contacts accepted by atoms O7 and O8 of the ***T***-oxalic ion are 44 and 41 kJ·mol^{-1}, respectively (Table S2).

In the crystal, the oxalate ions are linked with each other by O-H···O$^-$ hydrogen bonds to form infinite chains along the *b*-axis with C(5) graph set notation. Each chain contains oxalate conformers of one type only ("flat" or "twisted"). It is notable that the energy of the O5-H5···O7$^-$ bond (d(O5···O7$^-$) = 2.589 Å) in the chain of ***T***-oxalic ions is ~42 kJ·mol^{-1} (Figure 2a), while for the ***F***-oxalic ions the O1-H1···O4$^-$ bond reaches *ca.* 76 kJ·mol^{-1} (Figure 2b) (Table S2). The remarkably high electron density in the bond critical point for the latter interaction (ρ_b = 0.090 a.u.) and short O1···O4$^-$ distance (2.463 Å) indicate its partially covalent nature.[54] The stronger H-bonds between the flat oxalate anions compared to the twisted ones are possibly caused by the better charge delocalization in the ***F***-oxalic ions.

(a)

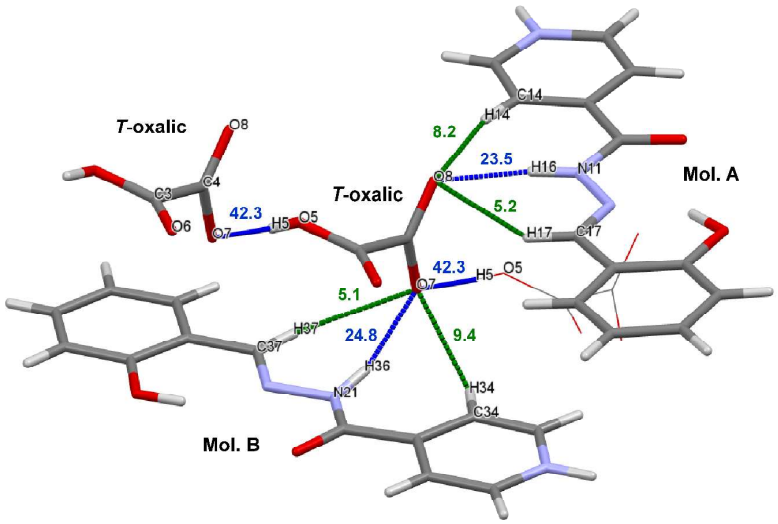

(**b**)

(**c**)

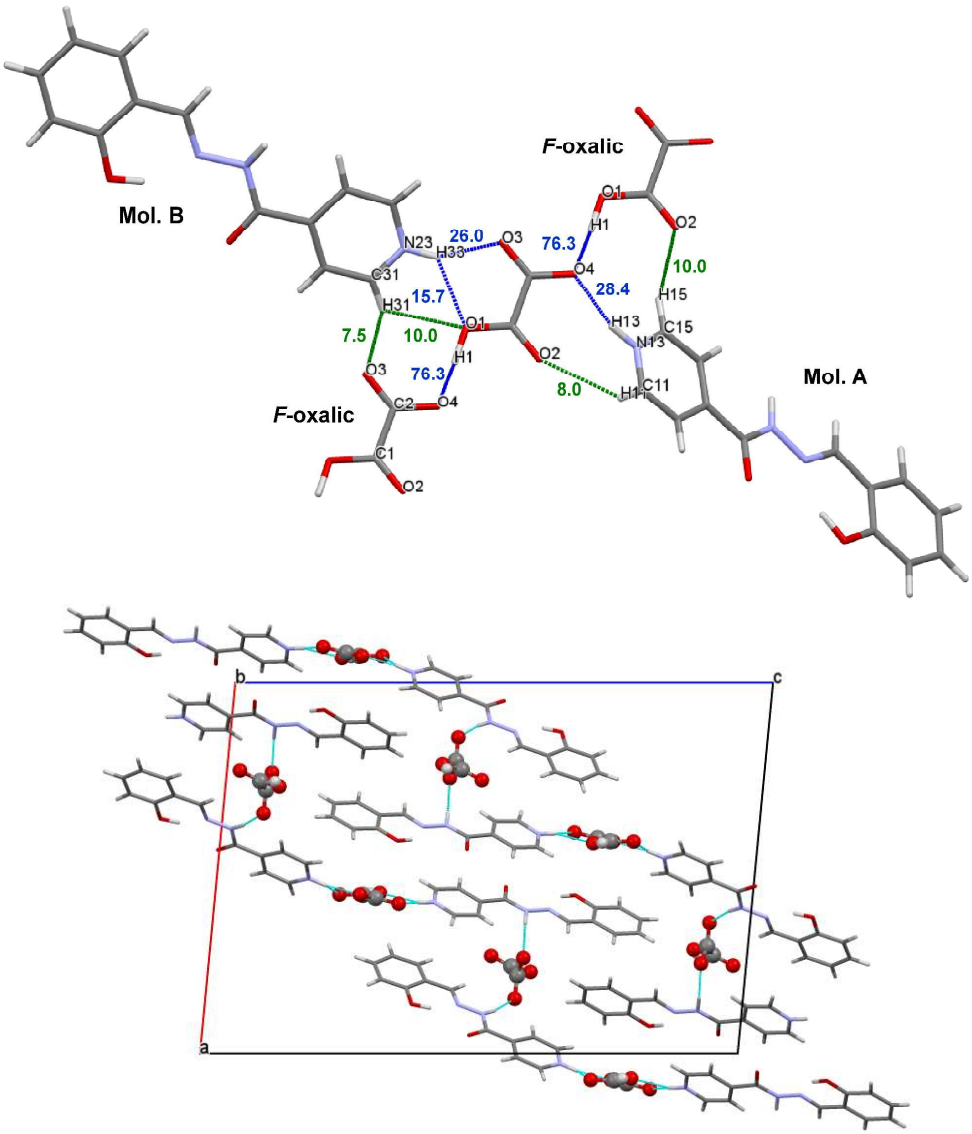

Figure 2. Intermolecular hydrogen bonds (blue) and C–H···O contacts (green) along the chain of (**a**) ***T***-anions of oxalic acid, (**b**) ***F***-anions of oxalic acid, (**c**) packing arrangement of the [**Slz**+**Oxalic**] salt along b-axis. The interaction energies are given in kJ·mol^{-1}.

The API and oxalic acid molecules do not form the expected acid-pyridine synthon, instead the ***F***-molecules of oxalic acid accept the bifurcated N23^{+}-H33···O3(O1) H-bonds from the protonated pyridine group of molecule **B**. In addition, N13^{+}-H13···O4^{-} bond links ***F***-oxalate ion and molecule **A** (Figure 2b). The energy of the N23^{+}-H33···O3 hydrogen bond (d(N23^{+}···O3) = 2.762 Å) is roughly equal to that of N13^{+}-H13···O4^{-} (d(N13^{+}···O4) = 2.758 Å) (26 versus 29

kJ·mol^{-1}) due to the charge delocalization in the deprotonated carboxylic group of the acid, while the N23^{+}-H33···O1 bond (d(N23^{+}···O1) = 2.862 Å) has only *ca.* 16 kJ·mol^{-1} (Table S2). It is interesting to note that QTAIMC analysis did not confirm the existence of the (3;-1) critical point corresponding to N13^{+}-H13···O2 contact, despite the fact that geometrical criteria (d(N13^{+}-O2) = 3.029 Å, ∠(N13^{+}-H13···O2) = 120.8°) suggest formation of a weak hydrogen bond. Considering the energy of several C-H···O contacts (Figure 2b), the strength of the oxalate-pyridinium synthons is estimated to be 52 kJ·mol^{-1} for the **B**-***F*** pair and 37 kJ·mol^{-1} for **A**-***F*** pair.

A number of the (3;-1) bond critical points corresponding to weak C–H···O contacts between the symmetry unequivalent salinazid molecules have been located by the QTAIMC analysis. The A molecules are arranged in centrosymmetric dimers interacting via the C12-H12...O11 (d(C12···O11) = 3.218 Å) and C11-H11...O12 (d(C11···O12) = 3.366 Å) contacts with a total E_{int} value of *ca.* 18 kJ·mol^{-1} (Figure S4a). In the case of **B** molecules, only weak C32-H32...O21 (d(C32···O21) = 3.530 Å) contacts ($E_{int} \approx 6$ kJ·mol^{-1}) are detected (Figure S4b).

In the [**Slz**+**Oxalic**] (1:1) crystal, different motifs of H-bonds are united into a complex chain consisting of salinazid and oxalate ions to form a distinct layer. The neighboring layers, however, are not hydrogen bonded to each other and interact only *via* C–H···O contacts and van der Waals forces (Figure 2c).

3.1.2 [**Slz**+**Malic**] (1:1)

In the crystal of the [**Slz**+**Malic**] (1:1) salt, the malate anions are assembled into C(7) chains by O21-H21···O24^{-} hydrogen bonds (d(O21···O24^{-}) = 2.634 Å), and each chain consists of one enantiomer only (Figure3a). The H-bonds between malate ions in chains are the strongest non-

covalent interactions in the crystal with the energy about 36 kJ·mol^{-1} (Table S3). In addition, malate ions of different chirality form $R_2^2(10)$ ring motifs through the O25–H25···O23 hydrogen bonds (d(O25···O23) = 2.841 Å) between the hydroxyl and carboxylic groups (*ca.* 25 kJ·mol^{-1}), connecting the neighboring chains into a single layer (Figure 3a). The pyridine nitrogen of **Slz** is involved in the relatively weak bifurcated N3^{+}–H3···O24^{-} (O25) bonds with the deprotonated carboxyl group and hydroxyl group of the malate ion (d(N3^{+}···O24^{-}) = 2.739 Å, d(N3^{+}···O25) = 3.002 Å) with *ca.* 27 and *ca.* 11 kJ·mol^{-1}, respectively (Figure 3b). This value is nearly equal to the energy of the **A-F** bifurcated synthon in the [**Slz**+**Oxalic**] (1:1) structure with similar topology (see Tables S2 and S3).

The O23 atom of the acid carboxylic group accepts the N1-H6···O23 (d(N1···O23) = 2.856 Å) bond from the hydrazide group of API, which brings additional 19 kJ·mol^{-1} to the API-acid interaction energy (Figure 3b). It has to be pointed out that, like in [**Slz**+**Oxalic**], the energy of acid-acid interactions in the crystal (*ca.* 61 kJ·mol^{-1}) is larger than acid-pyridine synthon energy (*ca.* 38 kJ·mol^{-1}), suggesting the structure-forming role of the acid chains in the salt.

The packing arrangement of the salt can be described as alternating layers of malate and salinazide ions in the (001) planes (Figure 3c). The layers are segregated so that there are clear regions with hydrogen bonding between **Slz** and malate ions and regions where only **Slz** molecules interact via van der Waals forces.

(**a**)

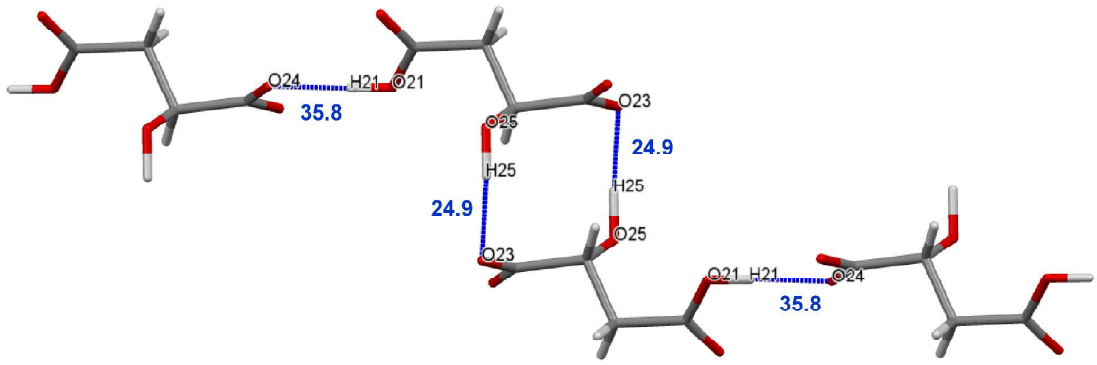

(**b**)

(**c**)

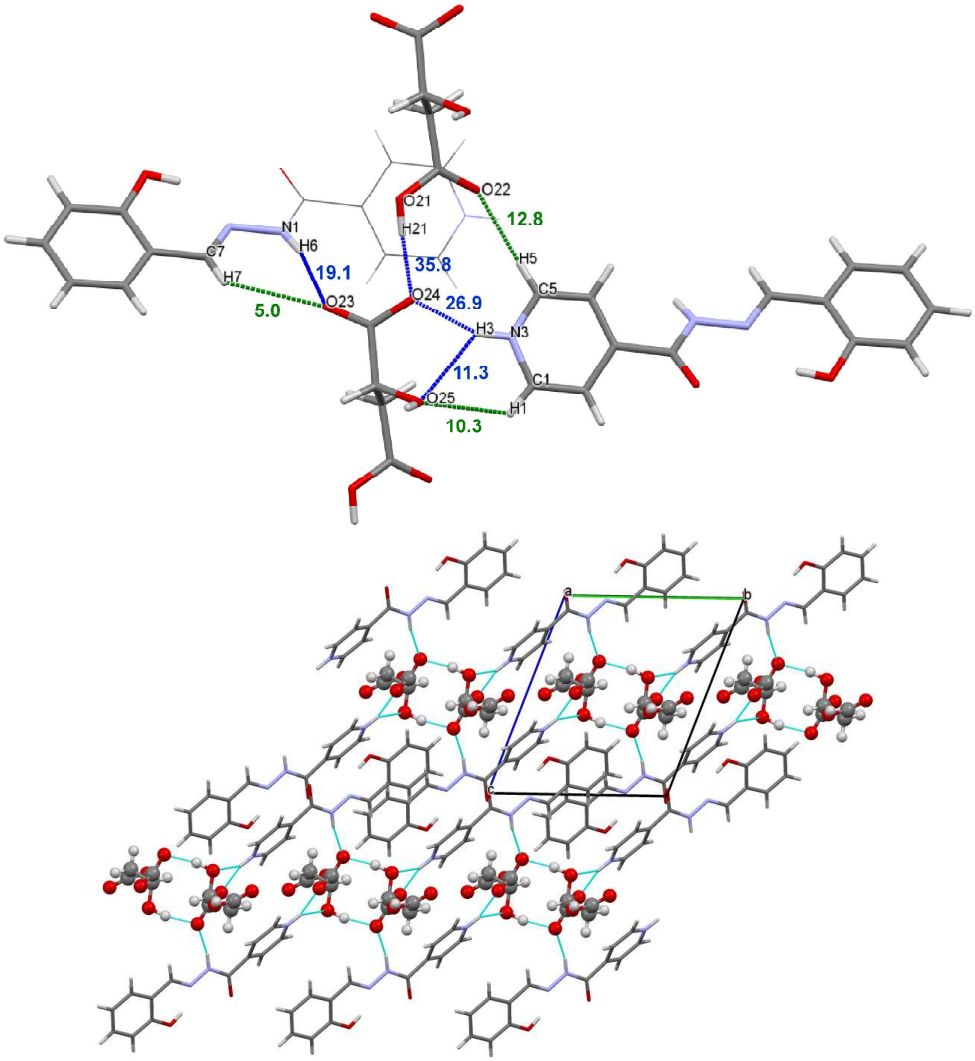

Figure 3. (**a**) Hydrogen bonded chain and ring motives between malate ions, (**b**) hydrogen bonds (blue) and C–H···O contacts (green) in the crystal of [**Slz**+**Malic**], (**c**) packing arrangement of the [**Slz**+**Malic**] salt along a-axis. The interaction energies are given in kJ·mol^{-1}.

3.1.3 [**Slz**+**Malonic**] (1:1)

The asymmetric unit of the [**Slz**+**Malonic**] (1:1) salt contains one **Slz** cation and one malonate anion linked by the charge assisted $N3^{+}$–H3···$O21^{-}$ hydrogen bond (d($N3^{+}$···$O21^{-}$) = 2.516 Å; E_{int} = 72 kJ·mol^{-1}), which is the strongest H-bond among all other hydrogen bonds present in the crystal structure (Table S4). This level of energy is in good agreement with the reported value for

3-hydroxypyridinium benzoate crystal, where a similar proton transfer forms an N^+–H···O bond.[38] The $N3^+$–H3···$O21^-$ H-bond, along with C5-H5···O22 contact, completes a nearly planar robust pyridinium-carboxylate heterosynthon ($R^2_2(7)$ in graph set notation) with the estimated energy of 78 kJ·mol^{-1} (Figure 4a).

Malonate ions are assembled into C(6) chains along the *c*-axis via O23-H23···$O21^-$ hydrogen bonds (d(O23···$O21^-$) = 2.624 Å) with moderate strength (ca. 36 kJ·mol^{-1}) (Figure 4a). Unlike the above discussed structures, the energy of acid-acid interactions in the crystal is significantly lower than that in the acid-pyridine synthon (36 against 78 kJ·mol^{-1}) (Table S4). It would be interesting to note that the strong affinity of **Slz** to malonic acid and the high vapor pressure of the latter may be the reason for spontaneous salt formation when two solids are simply brought in contact with one another[55] (see Figure S5). This effect was not observed (at least by the naked eye) for the systems with oxalic and malonic acids.

Another N1–H6···O22 hydrogen bond (d(N1···O22) = 2.926 Å) with energy *ca.* 19 kJ·mol^{-1} connects two neighboring [**Slz**+**Malonic**] units to form a C(11) hydrogen bonded chain along the *b*-axis (Table S4). The O22 atom also accepts two C4-H4···O22 and C7-H7···O22 contacts (d(C4···O22) = 3.260 Å; d(C7···O22) = 3.549 Å), which brings additional *ca.* 15 kJ·mol^{-1} (Figure 4a). In a chain, nearly planar [**Slz**+**Malonic**] units are packed in a perpendicular manner to form an angle of *ca* 88° to each other (Figure 4b). The neighboring units are additionally stabilized by the weak C5-H5···O1 contacts (≈ 9 kJ·mol^{-1}) between the **Slz** molecules (Figure S6a).

Combinations of different chain motifs result in formation of complex H-bonded rings including 30 or more atoms (not shown). In contrast to the [**Slz**+**Oxalic**] (1:1) and [**Slz**+**Malic**]

(1:1) crystals, the network of hydrogen bonds in [**Slz**+**Malonic**] (1:1) covers the entire crystal so that the components are linked to each other through various H-bond motifs.

(**a**)

(**b**)

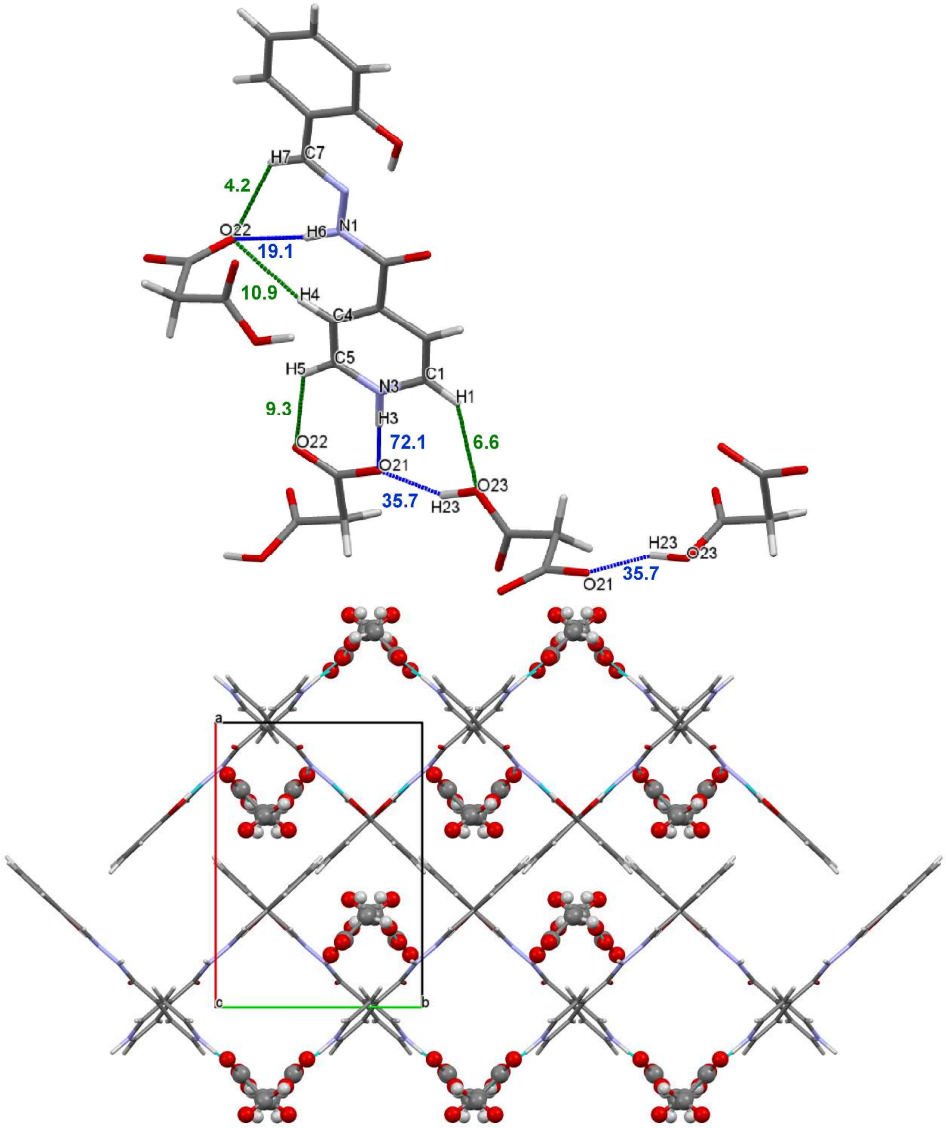

Figure 4. (**a**) Hydrogen bonds (blue) and main C–H···O contacts (green) in the crystal of [**Slz**+**Malonic**], (**b**) packing arrangement of the [**Slz**+**Malonic**] salt along c-axis. The interaction energies are given in kJ·mol^{-1}.

3.1.4 [**Slz**+**Acesulfame**]

The crystal structure of [**Slz**+**Acesulfame**] (1:1) is similar to that of the salinazid saccharinate salt reported by us previously.[9] In the asymmetric unit, **Slz** and acesulfame molecules are connected by a strong $N3^{+}$–H3···O6 hydrogen bond (d($N3^{+}$···O6) = 2.587 Å; E_{int} = 51 kJ·mol^{-1}) involving the pyridinium nitrogen of the API and the carbonyl oxygen atom of the oxathiazin ring of the salt former (Table S5). The relatively flat API and hydrogen-bonded acesulfame molecules lie approximately in the same plane to form a distinct unit (Figure 5a). The N1–H6···N4 hydrogen bond (d(N1···N4) = 2.587 Å) with E_{int} ≈ 17 kJ·mol^{-1} connects two neighboring [**Slz**+**Acesulfame**] units constructing a hydrogen bonded ribbon consisting of API and acesulfame ions, which is expended along the *b*-axis (Figure 5b). In the previously studied [**Slz**+**Saccharin**] (1:1) crystal, N1-H6 group and adjacent C-H groups of the API form non-covalent interactions with oxygen atoms of the SO_2 group of saccharin.[9] In the case of [**Slz**+**Acesulfame**] (1:1), this site of the **Slz** molecule interacts with N4, O4 and O6 atoms of acesulfame through the N1-H6···N4 bond as well as two C-H···O contacts of different strength (Figure 5a). These interactions taken all together contribute *ca.* 34 kJ·mol^{-1} to the lattice energy (Table S5).

Similar to the salinazid saccharinate crystal, [**Slz**+**Acesulfame**] units in a chain form an angle of *ca* 69° with each other. The chains are packed into layers in the crystallographic (100) planes, with the acesulfame ions pointing towards the layer surfaces (Figure 5b). Similar to the [**Slz**+**Malonic**] (1:1) crystal, the **Slz** molecules interact with each other via relatively strong C5-H5···O1 (d(C5···O1) = 3.040 Å) contacts (16 kJ·mol^{-1}) to form C(6) motifs (see Figure S6b).

(**a**)

(**b**)

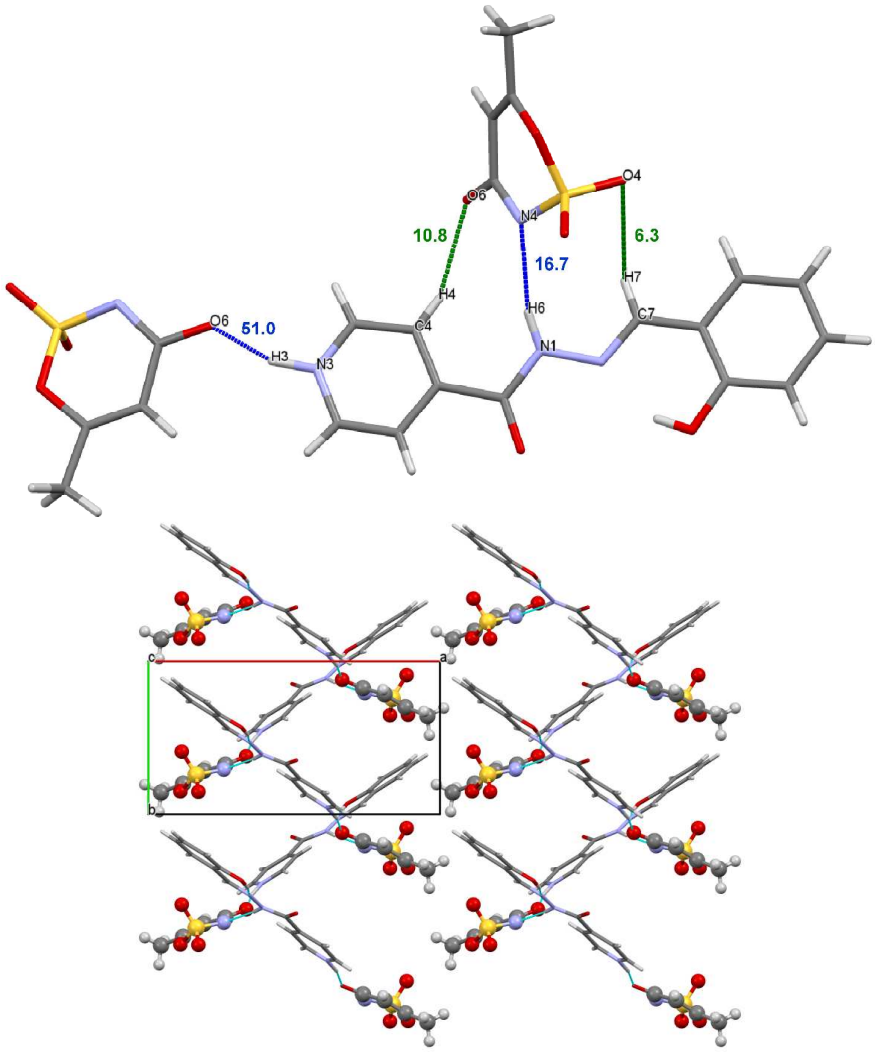

Figure 5. (**a**) Hydrogen bonds (blue) and main C–H···O contacts (green) in the crystal of [**Slz**+**Acesulfame**], (**b**) packing arrangement of the [**Slz**+**Acesulfame**] salt along c-axis. The interaction energies are given in kJ·mol^{-1}.

3.1.5 Concluding remarks on the salinazid salts with dicarboxylic acids.

The structure analysis has revealed that in the [**Slz**+**Oxalic**] (1:1), [**Slz**+**Malic**] (1:1) and [**Slz**+**Malonic**] (1:1) crystals, acid molecules tend to interact with each other via recurring chain motives of H-bonds. The main reason for that is most likely the 1:1 molar ratio between the API and acid molecules in crystals leaving one carboxylic group of the acid free to form hydrogen

bonds with surroundings. The QTAIMC analysis has confirmed that there is an energy preference behind the chain structure of H-bonds. In the [**Slz**+**Oxalic**] (1:1) crystal, the energy of acid-acid interactions is *ca.* 1.5 times stronger than the total energy of the bifurcated N^{+}–H···O hydrogen bonds between the API and acid ions. It is not surprising that a similar structure of the hydrogen bond network is also found in salts of oxalic acid with different weak pyridine bases, such as 4-(hydroxyiminomethyl)pyridinium hydrogen oxalate (COSDUK), pyridinium oxalate (DEFCUM), nicotinamidium oxalate (LICLEP), 4-aminopyridinium oxalate (MOSNAK), 2-amino-5-nitropyridinium oxalate (QOCCUI).

Combination of chain and bifurcated motifs is also typical for [**Slz**+**Malic**] (1:1) crystal. Malic acid has a hydrogen bonding site, the spatial geometry of which is essentially close to that in oxalic acid (Figure 6).

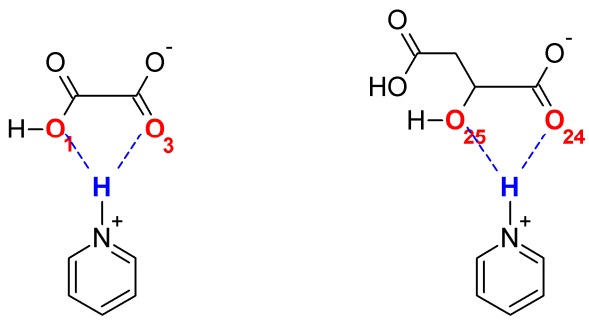

[**Slz**+**Oxalic**] [**Slz**+**Malic**]

Figure 6. Hydrogen bonding sites in the oxalate and malate ions

The $O24_{carboxyl}\cdots O25_{hydroxyl}$ distance in malic acid (2.728 Å) is comparable with the $O3_{carboxyl}\cdots O1_{carboxyl}$ distance in oxalic acid (2.649 Å), which probably explains the formation of similar bifurcated H-bonded synthons between the API and respective acid molecules.

In [**Slz**+**Malonic**] (1:1) the bifurcated H-bonded synthon cannot be formed between the API molecules and the acid due to sterical hindrances in malonic acid. Instead, the API and malonic

acid are connected by a stable pyridinium-carboxylate heterosynthon, which is the strongest non-covalent interaction in the crystal.

Therefore, in terms of energy hierarchy of the H-bonds, the [**Slz**+**Oxalic**] and [**Slz**+**Malic**] crystals may be considered as chains of acids to which the API molecules are attached. In the [**Slz**+**Malonic**] salt, however, the acid-acid H-bonded chains act as linkers of the API-acid pyridinium-carboxylate heterosynthons. This competition between different motifs of H-bonds is not trivial and hard to predict though, so additional studies of an extended set of salts are needed in order to clarify the structure-energy relationships.

3.2 Conformational analysis

The conformational state of the salinazid molecule can be described by using at least three torsion angles, namely τ_1 (∠C2-C3-C6-N1), τ_2, (∠C6-N1-N2-C7) and τ_3, (∠N2-C7-C8-C9) (see Figure 1). The torsion angles τ_1 and τ_3 are responsible for the rotation of the pyridine and phenyl rings, respectively. The torsion angle τ_2 defines the conformation of the central spacer unit between these two rings. The angle between the least-squares planes of the aromatic rings, β, was also taken in consideration.

Table 2. Selected torsion angles and dihedral angles between planes of aromatic rings, β, of salinazid molecule in different crystal forms.

	τ_1 (C2-C3-C6-N1),°	**τ_2 (C6-N1-N2-C7),°**	**τ_3 (N2-C7-C8-C9),°**	**β,°**
[**Slz**+**Oxalic**] (1:1) mol A	178.5 (C12-C13-C16-N11)	-177.2 (C16-N11-N12-C17)	-2.6 (N12-C17-C18-C19)	2.8
[**Slz**+**Oxalic**] (1:1) mol B	176.5 (C32-C33-C36-N21)	-174.6 (C36-N21-N22-C37)	-2.6 (N22-C37-C38-C39)	1.7
[**Slz**+**Malonic**] (1:1)	178.0	176.0	-4.0	10.9
[**Slz**+**Malic]** (1:1)	144.0	-177.2	4.9	30.2
[**Slz**+**Acesulfame]** (1:1)	-168.9	168.9	-0.3	4.0
[**Slz**+**Saccharin]** (1:1)	169.2	-175.35	7.90	3.4

Slz ion after geometry optimization[a]	157.1	174.6	0.6	30.2

[a]Geometric optimization for the salinazid ion was performed using the GAUSSIAN09 program at the B3LYP/6-311++G(d,p) level of theory.[56]

Table 2 indicates that conformational differences between the API molecules in the salts are small. The τ_2 torsion angle values change by no more than ±7º from 180º. Most of the τ_3 values are found to be close to 0º. The pyridine ring (τ_1) is mainly coplanar to the rest of the molecule. For [**Slz**+**Malic**] (1:1), however, the pyridine orientation is relatively further twisted from planarity, increasing the β values up to *ca* 30º.

In order to investigate conformational preferences of the API molecules, a search of the CSD (version 5.36, may 2015 update)[53] for crystal structures of N-isonicotinoyl arylaldehydehydrazones derivatives was performed. The search constraints were: 3-D coordinates were determined, only organics, no powder structures, not disordered, R < 0.1. As a result, 145 hits, including hydrates, solvates, salts and co-crystals, were retrieved and analyzed. The distribution of the τ_1, τ_2 and τ_3 torsion angles from the retrieved CSD set is described in the supporting information (Figures S7). Herein, we mainly focus on analysis of the dihedral angle between the planes of aromatic rings (β), which is an integral conformational characteristic and the most informative parameter to consider. Figure 7 shows that the distribution profile of β-parameter has a maximum at *ca* 9º, whereupon the occurrence frequency gradually decreases as β increases.

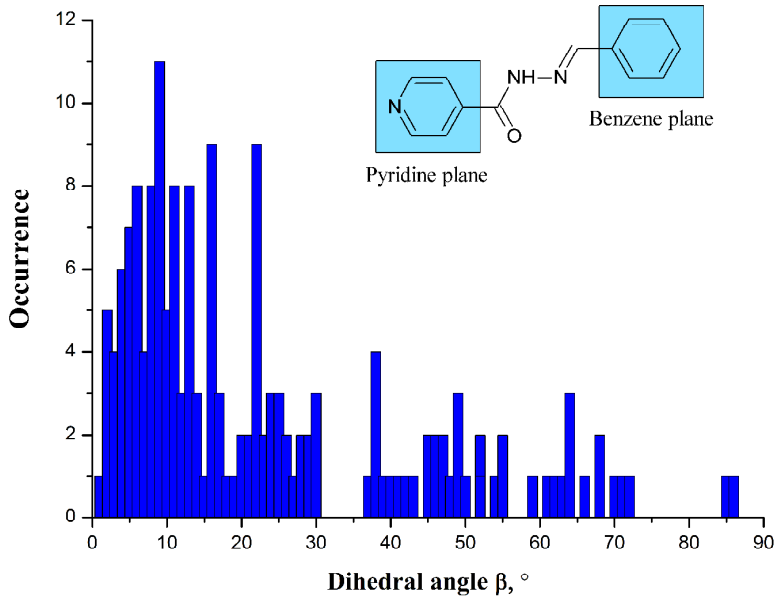

Figure 7. Distribution of dihedral angle between planes of aromatic rings, β, in N-isonicotinoyl arylaldehydehydrazone derivatives from retrieved CSD set (145 hits).

Most structures are located between 0 º and 30º, indicating that hydrazon derivatives tend to be flat in a crystal. The crystal structures of the salts described here are generally consistent with the populations obtained from the CSD survey. In the [**Slz**+**Malic**] (1:1) crystal, the API conformation is found to be close to the geometry of an isolated **Slz** ion (Table 2). This minimum-energy conformation, however, is rare in crystals, which suggests that conformation of hydrazon molecules is under the influence of supramolecular surroundings. The packing energy gained in the case of nearly planar geometry must be greater than the conformational energy penalty caused by the deviation of the molecule from its optimal geometry.

3.3 Thermal analysis.

Thermal stability of the salinazid salts was evaluated by the DSC method. The DSC results for the salts and pure salinazid are shown in Figure 8, and the thermal data are tabulated in Table 3.

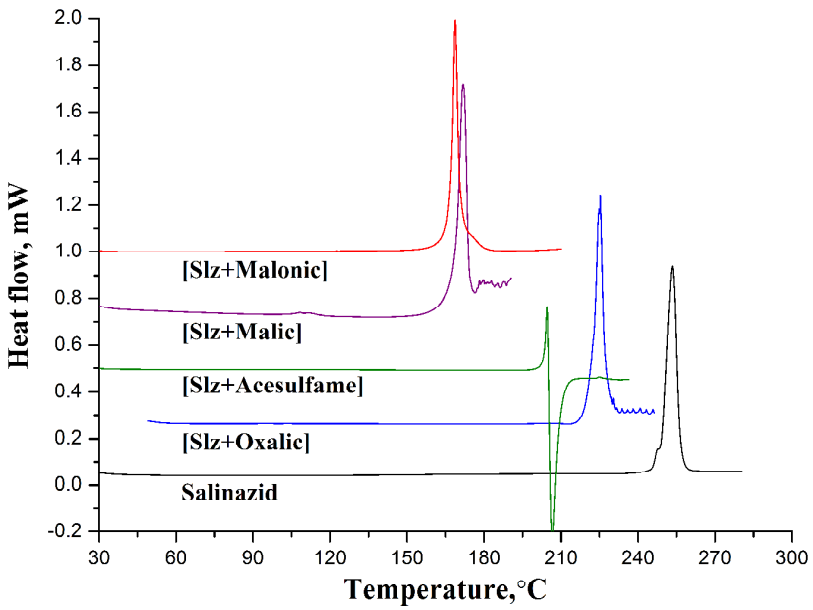

Figure 8. DSC curves of salinazid and corresponding salts recorded at 10 °C·min^{-1} heating rate.

Table 4. Thermophysical data for salinazid salts.

	T_{fus} (salt), °C (onset)	ΔH^{T}_{fus}, kJ·mol^{-1}[a]	T_{fus} (acid), °C
[**Slz**+**Oxalic**] (1:1)	221.2± 0.5	72.5 ± 1.6	189.0
[**Slz**+**Acesulfame**] (1:1)	202.2 ± 1.0	≈ 31	121.3
[**Slz**+**Malic**] (1:1)	169.7 ± 0.8	54.1 ± 2.0	130.6
[**Slz**+**Malonic**] (1:1)	162.6 ± 0.5	59.9 ± 1.5	135.2
[**Slz**+**Saccharin**] (1:1)[b]	195.8 ± 0.3	64.9 ± 1.0	227.0
Salinazid[b]	249.0 ± 0.4	42.5 ± 1.5	

[a]For the salts, the values correspond to a mole of molecules in the asymmetric unit.

[b]Data taken from ref. 9.

As Table 4 indicates, the melting temperatures for most of the salts are located in between the melting temperatures of respective pure components. An exception is seen only for salinazid saccharinate.[9] The [**Slz**+**Oxalic**] (1:1) salt demonstrates the largest thermal stability (221.2 °C), while the least T_{fus} values are observed in salinazid malate (169.7 °C) and salinazid malonate

(162.6 °C). Interestingly, the melting temperatures of these salts qualitatively correlate with the energy of O-H···O interactions between the respective acid ions in the salt crystals (see 3.1). This fact indicates that the acid-acid interactions in the crystals provide a significant impact to the thermal stability of the salts, altering the melting behavior of the API over a significant temperature range (≈60 °C).

The DSC curve of [**Slz**+**Acesulfame]** (1:1) demonstrates a sharp endothermic peak at 203°C, which is immediately followed by an intense exothermic peak indicating decomposition process of acesulfame. A similar thermal behavior has been observed for the acesulfame salts with 5-fluorocytosine[21] and co-crystal with griseofulvin.[19] Analysis of the salts thermal stability against melting points of the corresponding pure acids did not reveal any clear correlation. This, however, is not unexpected since the acids used are not structurally consistent.

3.4 Aqueous solubility and salts stability

Solubility and stability in aqueous media are the most important physicochemical properties to consider when preparing new solid forms of an API. The solubility values of salinazid and its salts in water at 25°C are shown in Figure 9 and tabulated in Table 5.

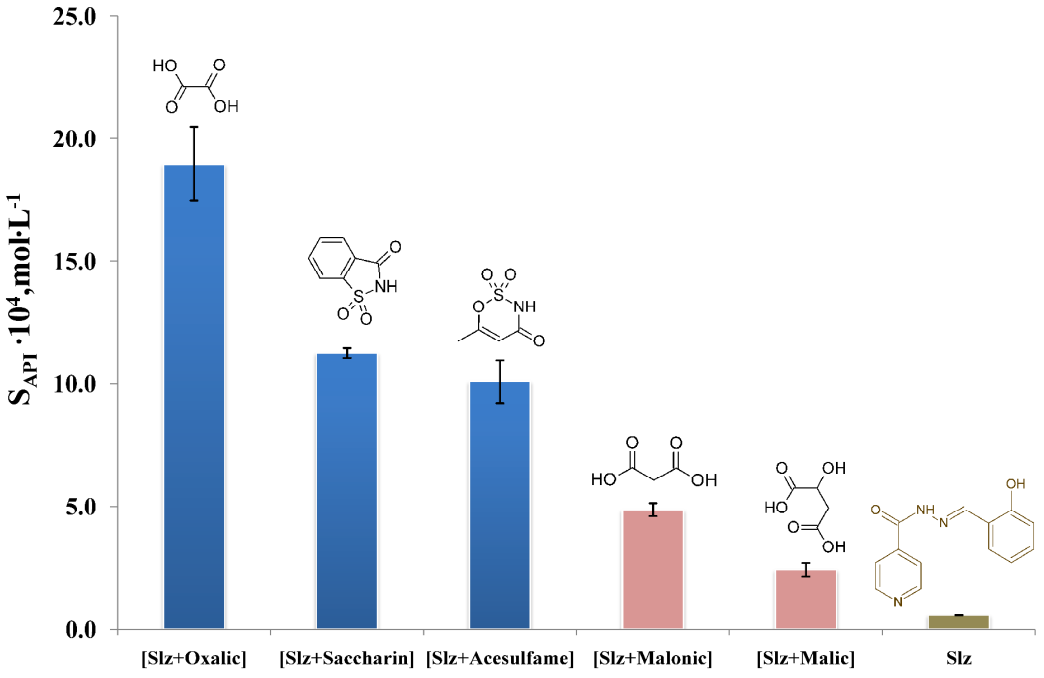

Figure 9. Solubility of the salinazid salts in water at 25°C. Stable salts are colored in blue. Unstable salts are colored in red. Solubility of pure salinazid is shown in brown color.

The largest concentration gain of API is observed during the dissolution of salinazid oxalate, which is found to be *ca.* 33 times more soluble than the parent drug. The [**Slz**+**Acesulfame**] (1:1) salt shows a relatively moderate 18-fold solubility enhancement in relation to pure API. This value is comparable to that for the salinazid saccharinate (20 times).[9] In general, the concentration level of salinazid decreases in the following order, [**Slz**+**Oxalic**] > [**Slz**+**Saccharine**] > [**Slz**+**Acesulfame**] > [**Slz**+**Malonic**] > [**Slz**+**Malic**] > **Slz**.

However, XRPD analysis of the residual material recovered after the experiment has revealed that only two salts, namely [**Slz**+**Oxalic**] (1:1) and [**Slz**+**Acesulfame**] (1:1), remain stable during the dissolution experiment (Figure S8 a,b). Whereas, the [**Slz**+**Malonic**] (1:1) and [**Slz**+**Malic**] (1:1) salts dissolve incongruently and undergo a solution-mediated transformation to form pure salinazid in the bottom phase (Figure S8 c,d).

For the stable salts, the free energy of formation in a particular solvent can be estimated be the following relation:[57]

$$\Delta G_f^0 = -RT \cdot \ln\left(\frac{10^{pK_{a,B}-pK_{a,A}} S_A^p \cdot S_B^p}{K_{sp}^{app}}\right) \quad (2)$$

where R is the gas constant, T is the temperature, K_{sp}^{app} is the apparent solubility product of the salt, S_A^p and S_B^p are the solubility of pure A and B in a solvent, $pK_{a,A}$ and $pK_{a,B}$ are dissociation constants of components. In order to ensure proximity of the intrinsic pK_a value of each compound and to attain consistency with the reported solubility data for the pure acids, all the solubility measurements were performed in an unbuffered water solution. It should be noted that K_{sp}^{app} is expressed in terms of concentration, with the approximation that the activity coefficient for all the species is 1.0, and the impact of the ionic strength on the activity coefficient of the solution is neglected.

Equation (2) also suggests that for a salt to be thermodynamically stable, the following condition has to be fulfilled:[58]

$$K_{sp}^{app} < 10^{pK_{a,B}-pK_{a,A}} S_A^p \cdot S_B^p \quad (3)$$

The numerical values for the right-hand and left-hand sides of equation (3) and the Gibbs energies of formation for the stable salinazid salts are shown in Table 5.

Table 5. Solubility of salts (S_{API}) and corresponding pure acids (S_{acid}), K_{sp} values and Gibbs energies of the salts formation in water at 25°C.

	$S_{API} \cdot 10^4$	S_{acid}	K_{sp}^{app}	$10^{pK_{a,B}-pK_{a,A}} S_A^p \cdot S_B^p$	ΔG_f^0	Stability
	$mol \cdot L^{-1}$	$mol \cdot L^{-1}$			$kJ \cdot mol^{-1}$	

[**Slz**+**Oxalic**] (1:1)[a]	19.0 ± 1.5	1.6[b]	$3.6\cdot10^{-6}$	$1.8\cdot10^{-2}$	-21.2	Stable
[**Slz**+**Acesulfame**] (1:1)[a]	10.1± 1.0	4.2[c]	$1.1\cdot10^{-6}$	$9.5\cdot10^{-3}$	-22.6	Stable
[**Slz**+**Saccharin**] (1:1)[a]	11.3 ± 0.2	$1.7\cdot10^{-2}$[d]	$1.3\cdot10^{-6}$	$2.4\cdot10^{-5}$	-7.3	Stable
[**Slz**+**Malic**] (1:1)	2.5 ± 0.3	4.4[b]	–	$4.0\cdot10^{-4}$	–	Unstable
[**Slz**+**Malonic**] (1:1)	4.8 ± 0.3	5.7[b]	–	$2.0\cdot10^{-3}$	–	Unstable
Salinazid	0.57±0.02[d]	–	–	–	–	–

[a]For the stable salts, the numbers represent concentration of each of API and acid in a stoichiometric solution in equilibrium with the salt.

[b]Data taken from the ref. 59.

[c]This work.

[d]Data taken from the ref. 9.

The K_{sp}^{app} values for the stable [**Slz**+**Oxalic**] (1:1) and [**Slz**+**Acesulfame]** (1:1) salts were calculated from the solubility experiments and found to be considerably smaller than the product of $10^{pK_{a,B}-pK_{a,A}} S_A^p \cdot S_B^p$. In addition, the Gibbs energies of formation of the salts derived from equation (2) were found to be more negative than that for [**Slz**+**Saccharine**] (1:1) (-7.3 kJ·mol^{-1}).[9] It suggests a greater thermodynamic stability of the [**Slz**+**Oxalic**] (1:1) and [**Slz**+**Acesulfame]** (1:1) salts in relation to salinazid saccharinate. It has to be pointed out that the free energy of formation for the acesulfame salt is *ca.* 3 times larger than that of saccharinate salt, despite the similarity in the packing arrangement of the crystals (see 3.1.4). This issue seems likely to be related to a considerable difference in the lattice free energy for pure acesulfame and saccharine. The difference can be qualitatively estimated by considering melting temperatures of the compounds: 121.3°C for acesulfame acid and 227.0°C for saccharine.

The dissociation of the [**Slz**+**Malonic**] (1:1) and [**Slz**+**Malic**] (1:1) salts in water occurs almost immediately. It was observed by changing color of the powders: from yellow for the salts to white for pure salinazid. Low stability of the respective salts in water indicates that they do not obey the condition (3).

It is known that the aqueous stability of salts of weak bases (or acids) is strongly depended on pH range. Whether or not the salt form is thermodynamically favored is determined by the pH of the surroundings of the drug relative to its pH_{max} (the pH of maximum solubility).[60,61] Therefore, the difference in stability of the salinazid salts is related to the acid-base properties of the corresponding acids. The presence of the relatively strong acids (oxalic acid, acesulfame and saccharine) resulted in the solution pH (≈ 2.0) which is less than the pH_{max} value for the API compound.[6] As a result, the equilibrium between the solid phase and the solution is sustained and determined by K_{sp}^{app}, giving long-term solubility enhancement of the drug.

Malonic and malic acids, however, are too weak to provide the condition for the salts stability (pH < pHmax) in an unbuffered water solution due to their incomplete dissociation, which leads to rapid disproportionation of the salts. Despite the fact that in the presence of crystalline environment, the API and acid molecules are linked with each other via strong charge assisted hydrogen bonds. XRPD analysis of the residual materials after the solubility experiments suggests that salinazid precipitates to form a bottom phase, while the well-soluble acids pass into a water solution. Thus, the observed solubilization of the API in this case (Figure 9) should mainly be attributed to solution pH decrease due to the common effect of the carboxylate anions. In order to illustrate the influence of malonic and malic acids on the salinazid water solubility and verify the results of the dissolution study, phase solubility diagrams at 25ºC were constructed (Figure S9 of the Supporting Information). It is evident that as the acid concentration increases, the solution pH decreases and the concentration of the ionized form increases, leading to an increase in the total solubility of the API. However, transformation of the bottom phase during the experiment was not observed. Thus, an additional pH justification of the solution is needed to achieve the condition for K_{sp} determination of the malonate and malate salts.[62]

It can be concluded that the malonate and malate salts of salinazid have only minor interest in terms of their practical application due to low stability and poor solubility performance. On the other hand, our preliminary results suggest that the [**Slz**+**Oxalic**] (1:1), [**Slz**+**Acesulfame**] (1:1) and [**Slz**+**Saccharin**] (1:1) salts are promising solid forms to explore the diverse therapeutic potential of the API.

4. Conclusions

Novel salts of the biologically active hydrazone compound called salinazid with dicarboxylic acids and acesulfame have been obtained and their crystal structures have been determined. The crystals contain hydrogen bond motifs of different structure and complexity, the energies in which have been estimated by the QTAIMC analysis of the periodic electron density calculated by the solid-state DFT methods. The strongest H-bonds are found to form in the [**Slz**+**Oxalic**] (1:1) and [**Slz**+**Malic**] (1:1) crystals in the chains consisting of respective acid ions. Whereas, the API and acid molecules interact by forming bifurcated N^{+}–H···O^{-} and N^{+}–H···O synthons with the energy which is ca. 1.5-2 times lower than that for the acid-acid interactions. The alternative structure of H-bonds is observed in the [**Slz**+**Malonic**] (1:1) salt where the API and acid molecules are connected via a "classic" pyridinium-carboxylate heterosynthon, which is calculated to be the strongest hydrogen bonded motif among all other hydrogen bonds present in the crystal structure. Therefore, in terms of the energy hierarchy of the H-bonds, the [**Slz**+**Oxalic**] (1:1) and [**Slz**+**Malic**] (1:1) crystals may be considered to be chains of acids to which the API molecules are attached. In the [**Slz**+**Malonic**] (1:1) salt, however, the acid-acid H-bonded chains act as linkers of the API-acid pyridinium-carboxylate heterosynthons. For the [**Slz**+**Acesulfame**] (1:1) salt, the pattern and energy values of H-bonds are found to be similar to that for salinazid saccharinate reported by us previously.

The [**Slz**+**Oxalic**] (1:1) and [**Slz**+**Acesulfame**] (1:1) salts were found to be stable during aqueous dissolution experiments, providing a substantial solubility improvement compared to pure API (33 and 18 times, respectively). However, the [**Slz**+**Malonic**] (1:1) and [**Slz**+**Malic**] (1:1) salts dissolved incongruently and rapidly underwent a solution-mediated transformation to form pure salinazid, despite the fact that in the presence of crystalline environment, the API and acid molecules are linked with each other via strong charge assisted hydrogen bonds. Free energies of the formation of the stable salts were estimated based on their solubilities in water. For [**Slz**+**Oxalic**] (1:1) and [**Slz**+**Acesulfame**] (1:1), the values of the Gibbs energy change were found to be -21.2 $kJ \cdot mol^{-1}$ and -22.6 $kJ \cdot mol^{-1}$, respectively.

In conclusion, the relationship and correlation between the crystal structure and solubility is not a straightforward question, particularly then it deals with multicomponent crystals. It is known that the solubility of a compound is determined by a balance between its lattice energy (intermolecular interactions) and solvation energy (solute-solvent interactions). In certain cases, this balance is considerably shifted to the lattice energy side. Then, clear connection between crystal structure and solubility outcome can be established. In addition, such correlations are usually observed for the structurally related multicomponent crystals using, for example, cocrystals or salts of an API with homologous series of coformers. In our work, however, the salts under study show diversity of packing arrangements and intermolecular interactions. Moreover, the salt formers (acids) used have different acid-base properties and chemical structure. Therefore, it was hard to reveal evident link between the crystal structures of the salts and their solubility based on only five systems. Additional studies of an extended set of salts are needed in order to clarify this structure-property relationship.

Associated content

Supporting Information. Complete tables of geometrical and electron density parameters; the energy of the strongest noncovalent interactions in the salt crystals; results of conformational analysis for oxalate ion and N-isonicotinoyl arylaldehydehydrazones derivatives; XRPD patterns of the residual materials after the salts solubility; crystallographic data for hydrated salt of salinazid with monomethyl oxalate. The information is available free of charge via the Internet at http://pubs.acs.org.

Acknowledgements

This work was supported by a grant from the President of the Russian Federation no. MK-67.2014.3 and Russian Foundation for Basic Research (project № 14-03-31001). X-ray diffraction studies were performed at the Centre of Shared Equipment of IGIC RAS. We thank ‘‘The Upper Volga Region Centre of Physicochemical Research’’ for the technical assistance of XRPD experiments.

References

1. Davies, G. Changing the salt, changing the drug. *Pharm. J.* **2009**, *266*, 322–323.

2. Peterson, M. L.; Morissette, S. L.; Remenar, J. F.; Read, M. J.; Lemmo, A. V; Ellis, S.; Cima, M. J.; Gardner, C. R. High-throughput crystallization: polymorphs, salts, co-crystals and solvates of pharmaceutical solids. *Adv. Drug Delivery Rev.* **2004**, *56*, 275–300.

3. Rodriguez-Spong, B.; Price, C.P.; Jayasankar, A.; Matzger, A.J.; Rodriguez-Hornedo, N. General Principles of Pharmaceutical Solid Polymorphism: A Supramolecular Perspective. *Adv. Drug Deliv. Rev.* **2004**, *56*, 241–274.

4. Vippagunta, S. R.; Brittain, H. G.; Grant, D. J. W. Crystalline solids. *Adv. Drug Delivery Rev.* **2001**, *48*, 3-26.

5. Byrn, S. R.; Pfeiffer, R. R.; Stowell, J. G. *Solid-State Chemistry of Drugs*, 2nd ed.; SSCI Inc.: West Lafayette, IN, 1999.

6. Stahl, P. H., Wermuth, C. G., Eds. *Handbook of pharmaceutical salts, properties, selection and use*; Wiley-VCH: Weinheim, Germany, 2002.

7. Li, S.; Wong, S.; Sethia, S.; Almoazen, H.; Joshi, Y. M.; Serajuddin, A. T. Investigation of solubility and dissolution of a free base and two different salt forms as a function of pH. *Pharm. Res.* **2005**, *22*, 628−635.

8. Wouters, J.; Quere, L., Eds. *Pharmaceutical Salts and Co-Crystals*; Royal Society of Chemistry: London, 2011.

9. Surov, A. O.; Voronin, A. P.; Simagina, A. A.; Churakov, A. V.; Skachilova, S. Y.; Perlovich, G. L. Saccharin Salts of Biologically Active Hydrazone Derivatives. *New J. Chem.* **2015**, *39*, 8614–8622.

10. Rollas, S.; Küçükgüzel, Ş. G. Biological Activities of Hydrazone Derivatives. *Molecules* **2007**, *12*, 1910–1939.

11. Narang, R.; Narasimhan, B.; Sharma, S. A Review on Biological Activities and Chemical Synthesis of Hydrazide Derivatives. *Curr. Med. Chem.* **2012**, *19*, 569–612.

12. Vavříková, E.; Polanc, S.; Kočevar, M.; Košmrlj, J.; Horváti, K.; Bsze, S.; Stolaříková, J.; Imramovský, A.; Vinšová, J. New Series of Isoniazid Hydrazones Linked with Electron-Withdrawing Substituents. *Eur. J. Med. Chem.* **2011**, *46*, 5902–5909.

13. Martins, F.; Santos, S.; Ventura, C.; Elvas-Leitão, R.; Santos, L.; Vitorino, S.; Reis, M.; Miranda, V.; Correia, H. F.; Aires-de-Sousa, J.; Kovalishyn, V.; Latino, D. a. R. S.; Ramos, J.; Viveiros, M. Design, Synthesis and Biological Evaluation of Novel Isoniazid Derivatives with Potent Antitubercular Activity. *Eur. J. Med. Chem.* **2014**, *81*, 119–138.

14. Maccari, R.; Ottanà, R.; Vigorita, M. G. In Vitro Advanced Antimycobacterial Screening of Isoniazid-Related Hydrazones, Hydrazides and Cyanoboranes: Part 14. *Bioorg. Med. Chem. Lett.* **2005**, *15*, 2509–2513.

15. Buu-Hoi, P. H.; Xuong, D.; Nam, H.; Binon, F.; Royer, R. 278. Tuberculostatic hydrazides and their derivatives *J. Chem. Soc.* **1953***, 75,* 1358-1364.

16. Vanucci-Bacqué, C.; Carayon, C.; Bernis, C.; Camare, C.; Nègre-Salvayre, A.; Bedos-Belval, F.; Baltas, M. Synthesis, Antioxidant and Cytoprotective Evaluation of Potential Antiatherogenic Phenolic Hydrazones. A Structure-Activity Relationship Insight. *Bioorg. Med. Chem.* **2014**, *22*, 4269–4276.

17. Rodrigues, F. A. R.; Oliveira, A. C. A.; Cavalcanti, B. C.; Pessoa, C.; Pinheiro, A. C.; M. de Souza, V. N. Biological Evaluation of Isoniazid Derivatives as an Anticancer Class. *Sci. Pharm.* **2014**, *82*, 21–28.

18. Burgard, A. U.S. patents US2002/0197381A1 and US2005/6849623B2.

19. Aitipamula, S.; Vangala, V. R.; Chow, P. S.; Tan, R. B. H. Cocrystal Hydrate of an Antifungal Drug, Griseofulvin, with Promising Physicochemical Properties. *Cryst. Growth Des.* **2012,** 12, 5858−5863.

20. Aitipamula, S.; Wong, A. B. H.; Chow, P. S.; Tan, R. B. H. Pharmaceutical Salts of Haloperidol with Some Carboxylic Acids and Artificial Sweeteners: Hydrate Formation, Polymorphism, and Physicochemical Properties. *Cryst. Growth Des.* **2014**, *14*, 2542–2556.

21. Lin Wang, Xiaonan Wen, Ping Li, Jianming Wang, Ping Yang, H. Z. and Z. D. 2 : 1 5-Fluorocytosine–acesulfame CAB Cocrystal and 1 : 1 5-Fluorocytosine–acesulfame Salt Hydrate with Enhanced Stability against Hydratio. *CrystEngComm* **2014**, *16*, 8537–8545.

22. Wang, L.; Luo, M.; Li, J.; Wang, J.; Zhang, H.; Deng, Z. Sweet Theophylline Cocrystal with Two Tautomers of Acesulfame. *Cryst. Growth Des.*, **2015**, 15, 2574–2578.

23. Basavoju, S.; Bostrom, D.; Velaga, S. P. Pharmaceutical Salts of Fluoroquinolone Antibacterial Drugs with Acesulfame Sweetener. *Mol. Cryst. Liq. Crystals* **2012**, *562*, 254–264.

24. Velaga, S. P.; Vangala, V. R.; Basavoju, S.; Boström, D. Polymorphism in Acesulfame Sweetener: Structure–property and Stability Relationships of Bending and Brittle Crystals. *Chem. Commun.* **2010**, *46*, 3562-3564.

25. Sheldrick, G. M. A short history of *SHELX. Acta Crystallogr., Sect. A: Found. Crystallogr.*, **2007**, *64*, 112- 122.

26. Sheldrick, G. M. SADABS, Program for scaling and correction of area detector data. University of Göttingen, **1997**, Germany.

27. Higuchi, T.; Connors, K.A. Phase-solubility techniques. *Adv. Anal. Chem. Instrum*. **1965**, *4*, 117–212.

28. Dovesi, R.; Orlando, R.; Erba, A.; Zicovich-Wilson, C. M.; Civalleri, B.; Casassa, S.; Maschio, L.; Ferrabone, M.; De La Pierre, M.; D'Arco, P.; Noël, Y.; Causà, M.; Rérat, M.; Kirtman, B. CRYSTAL14 : A Program for the *ab Initio* Investigation of Crystalline Solids. *Int. J. Quantum Chem.* **2014**, *114*, 1287–1317.

29. Vener, M. V.; Manaev, A. V.; Egorova, A. N.; Tsirelson, V. G. QTAIM Study of Strong H-Bonds with the O-H···A Fragment (A = O, N) in Three-Dimensional Periodical Crystals. *J. Phys. Chem. A* **2007**, *111*, 1155–1162.

30. Munshi, P.; Row, T. N. G. Exploring the Lower Limit in Hydrogen Bonds: Analysis of Weak C-H···O and C-H···π Interactions in Substituted Coumarins from Charge Density Analysis. *J. Phys. Chem. A* **2005**, *109*, 659-672.

31. Nelyubina, Y. V; Glukhov, I. V; Antipin, M. Y.; Lyssenko, K. A. "Higher Density Does Not Mean Higher Stability" Mystery of Paracetamol Finally Unraveled. *Chem. Commun.* **2010**, *46*, 3469–3471.

32. Gatti, C.; Saunders, V. R.; Roetti, C. Crystal field effects on the topological properties of the electron density in molecular crystals. The case of urea. *J. Chem. Phys.*, **1994**, *101*, 10686-10696.

33. Tsirelson, V. G. The mapping of electronic energy distributions using experimental electron density. *Acta Cryst., Sect. B: Structural Science*, **2002**, *58*, 632-639.

34. Mata, I.; Alkorta, I.; Espinosa, E.; Molins, E. Relationships between interaction energy, intermolecular distance and electron density properties in hydrogen bonded complexes under external electric fields. *Chem. Phys. Lett.* **2011**, *507*, 185–189.

35. Vener, M. V.; Egorova, A. N.; Churakov, A. V.; Tsirelson, V. G. Intermolecular Hydrogen Bond Energies in Crystals Evaluated Using Electron Density Properties: DFT Computations with Periodic Boundary Conditions. *J. Comp. Chem.* **2012**, *33*, 2303–2309.

36. Vener M.V.; Shishkina, A. V.; Rykounov, A. A.; Tsirelson, V. G. Cl···Cl Interactions in Molecular Crystals: Insights from the Theoretical Charge Density Analysis, *J. Phys. Chem. A*, **2013**, *117*, 8459−8467.

37. Shishkina, A. V.; Zhurov, V. V.; Stash, A. I.; Vener, M. V.; Pinkerton, A. A.; Tsirelson, V. G. Noncovalent Interactions in Crystalline Picolinic Acid N-Oxide: Insights from Experimental and Theoretical Charge Density Analysis. *Cryst. Growth Des*. **2013**, *13*, 816 – 828;

38. Vener, M. V.; Levina, E. O.; Koloskov, O. a.; Rykounov, A. A.; Voronin, A. P.; Tsirelson, V. G. Evaluation of the Lattice Energy of the Two-Component Molecular Crystals Using Solid-State DFT. *Cryst. Growth Des.* **2014**, *14*, 4997-5003.

39. Katsyuba, S. A.; Vener, M. V.; Zvereva, E. E.; Fei, Z.; Scopelliti, R.; Brandenburg, J. G.; Siankevich, S.; Dyson, P. J. Quantification of Conventional and Nonconventional Charge-Assisted Hydrogen Bonds in the Condensed and Gas Phases. *J. Phys. Chem. Lett.* **2015**, DOI: 10.1021/acs.jpclett.5b02175.

40. Bhogala, B. R.; Basavoju, S.; Nangia, A. Tape and Layer Structures in Cocrystals of Some Di- and Tricarboxylic Acids with 4,4′-Bipyridines and Isonicotinamide. From Binary to Ternary Cocrystals. *CrystEngComm* **2005**, *7*, 551-562.

41. Childs, S.L.; Stahly, G.P.; Park, A. The Salt-Cocrystal Continuum: the Influence of Crystal Structure on Ionization State. *Mol. Pharmaceutics* **2007**, *4*, 323-338.

42. Cruz-Cabeza, A.J. Acid-Base Crystalline Complexes and the pKa Rule. *CrystEngComm* **2012**, *14*, 6362-6365.

43. Advanced Chemistry Development (ACD/Laboratories) Software V11.02.

44. Sarma, B.; Nath, N. K.; Bhogala, B. R.; Nangia, A. Synthon Competition and Cooperation in Molecular Salts of Hydroxybenzoic Acids and Aminopyridines. *Cryst. Growth Des.* **2009**, *9*, 1546–1557.

45. Mukherjee, A.; Desiraju, G. R. Combinatorial Exploration of the Structural Landscape of Acid–Pyridine Cocrystals. *Cryst. Growth Des.* **2014**, *14*, 1375–1385.

46. Aakeröy, C. B., Hussain, I., Desper, J. 2-Acetaminopyridine: A Highly Effective Cocrystallizing Agent. *Cryst. Growth Des.* **2006**, *6*, 474–480.

47. Bis, J. A.; Zaworotko, M. J. The 2-Aminopyridinium-Carboxylate Supramolecular Heterosynthon: A Robust Motif for Generation of Multiple-Component Crystals. *Cryst. Growth Des.* **2005**, *5*, 1169–1179.

48. Stahly, G. P. Diversity in Single- and Multiple-Component Crystals. The Search for and Prevalence of Polymorphs and Cocrystals. *Cryst. Growth Des.* **2007**, *7*, 1007–1026.

49. Steiner, T.; Majerz, I.; Wilson, C. C. First O-H-N Hydrogen Bond with a Centered Proton Obtained by Thermally Induced Proton Migration. *Angew. Chem. Int. Ed.* **2001**, *4*, 2651–2654.

50. Vener, M. V.; Egorova, A. N.; Fomin, D. P.; Tsirelson, V. G. Hierarchy of the non-covalent interactions in the alanine-based secondary structures. DFT study of the frequency shifts and electron-density features. *J. Phys. Org. Chem*., **2009**, *22*, 177–185.

51. Bader, R. F. W. *Atoms in Molecules - A Quantum Theory*; Oxford University Press: Oxford, 1990.

52. Tsirelson, V. G. *Interpretation of the Experimental Electron Densities by Combination of the QTAIM and DFT*. In *The Quantum Theory of Atoms in Molecules: From Solid State to DNA and Drug Design*. Matta, C.; Boyd, R. Eds.; Wiley-VCH; Berlin, 2007.

53. Allen, F. H. The Cambridge Structural Database: a quarter of a million crystal structures and rising. *Acta Crystallogr. B*. **2002**, *B58*, 380-388.

54. Gatti, C. Chemical Bonding in Crystals: New Directions. *Zeitschrift fur Krist.* **2005**, *220*, 399–457.

55. Chadwick, K.; Davey, R.; Cross, W. How Does Grinding Produce Co-Crystals? Insights from the Case of Benzophenone and Diphenylamine. *CrystEngComm* **2007**, *9*, 732-734.

56. Frisch, M. J.; Trucks, G. W.; Schlegel, H. B.; Scuseria, G. E.; Robb, M. A.; Cheeseman, J. R.; Scalmani, G.; Barone, V.; Mennucci, B.; Petersson, G. A.; et al. Gaussian 09, Revision C.01; Gaussian, Inc.: Wallingford CT, 2009.

57. Rager, T.; Hilfiker, R. Stability Domains of Multi-Component Crystals in Ternary Phase Diagrams. *Zeitschrift für Phys. Chemie* **2009**, *223*, 793–813.

58. Paluch, K. J.; Mccabe, T.; Mu, H.; Corrigan, O. I.; Healy, A. M.; Tajber, L. Formation and Physicochemical Properties of Crystalline and Amorphous Salts with Different Stoichiometries Formed between Ciprofloxacin and Succinic Acid. *Mol. Pharm.* **2013**, *10*, 3640–3654.

59. Yalkowsky, S. H.; He, Y.; Jain, P. *Handbook of Aqueous Solubility Data, Second Edition*; CRC Press: Boca Raton, 2010.

60. Stephenson, G. A.; Aburub, A.; Woods, T. A. Physical Stability of Salts of Weak Bases in the Solid-State. *J. Pharm. Sci.* **2011**, *100*, 1607–1617.

61. Elder, D. P.; Holm, R.; De Diego, H. L. Use of Pharmaceutical Salts and Cocrystals to Address the Issue of Poor Solubility. *Int. J. Pharm.* **2013**, *453*, 88–100.

62. Chiang, P. C.; South, S. A.; Daniels, J. S.; Anderson, D. R.; Wene, S. P.; Albin, L. A.; Mourey, R. J.; Selbo, J. G. Aqueous versus Non-Aqueous Salt Delivery Strategies to Enhance Oral Bioavailability of a Mitogen-Activated Protein Kinase-Activated Protein Kinase (mk-2) Inhibitor in Rats. *J. Pharm. Sci.* **2009**, *98*, 248–256.

For Table of Contents Use Only

Pharmaceutical salts of biologically active hydrazone compound salinazid: crystallographic, solubility and thermodynamic aspects

Artem O. Surov, Alexander P. Voronin, Anna A. Simagina, Andrei V. Churakov, German L. Perlovich

Salts of the biologically active hydrazone compound called salinazid with dicarboxylic acids and acesulfame were obtained, and their crystal structures were determined. The intermolecular interactions in the crystals were described by solid-state DFT complemented with the Bader analysis of periodic electron density. Solubility, stability and thermodynamics of the salts formation in water were investigated.